



AFRL-RQ-WP-TP-2013-0273

**ERROR QUANTIFICATION AND CONFIDENCE
ASSESSMENT OF AEROTHERMAL MODEL
PREDICTIONS FOR HYPERSONIC AIRCRAFT
(PREPRINT)**

Benjamin P. Smarslok and Adam J. Culler

**Hypersonic Sciences Branch
High Speed Systems Division**

Sankaran Mahadevan

Vanderbilt University

SEPTEMBER 2013

Approved for public release; distribution unlimited.

See additional restrictions described on inside pages

STINFO COPY

**AIR FORCE RESEARCH LABORATORY
AEROSPACE SYSTEMS DIRECTORATE
WRIGHT-PATTERSON AIR FORCE BASE, OH 45433-7542
AIR FORCE MATERIEL COMMAND
UNITED STATES AIR FORCE**

NOTICE AND SIGNATURE PAGE

Using Government drawings, specifications, or other data included in this document for any purpose other than Government procurement does not in any way obligate the U.S. Government. The fact that the Government formulated or supplied the drawings, specifications, or other data does not license the holder or any other person or corporation; or convey any rights or permission to manufacture, use, or sell any patented invention that may relate to them.

This report was cleared for public release by the USAF 88th Air Base Wing (88 ABW) Public Affairs Office (PAO) and is available to the general public, including foreign nationals.

Copies may be obtained from the Defense Technical Information Center (DTIC)
(<http://www.dtic.mil>).

AFRL-RQ-WP-TP-2013-0273 HAS BEEN REVIEWED AND IS APPROVED FOR PUBLICATION IN ACCORDANCE WITH ASSIGNED DISTRIBUTION STATEMENT.

**//Signature//*

BENJAMIN P. SMARSLOK
Project Manager
Hypersonic Sciences Branch
High Speed Systems Division

//Signature//

MARK AMENDT, Chief
Hypersonic Sciences Branch
High Speed Systems Division
Aerospace Systems Directorate

This report is published in the interest of scientific and technical information exchange, and its publication does not constitute the Government's approval or disapproval of its ideas or findings.

Disseminated copies will show "//Signature//*" stamped or typed above the signature blocks.

REPORT DOCUMENTATION PAGE				<i>Form Approved</i> OMB No. 0704-0188	
<p>The public reporting burden for this collection of information is estimated to average 1 hour per response, including the time for reviewing instructions, searching existing data sources, gathering and maintaining the data needed, and completing and reviewing the collection of information. Send comments regarding this burden estimate or any other aspect of this collection of information, including suggestions for reducing this burden, to Department of Defense, Washington Headquarters Services, Directorate for Information Operations and Reports (0704-0188), 1215 Jefferson Davis Highway, Suite 1204, Arlington, VA 22202-4302. Respondents should be aware that notwithstanding any other provision of law, no person shall be subject to any penalty for failing to comply with a collection of information if it does not display a currently valid OMB control number. PLEASE DO NOT RETURN YOUR FORM TO THE ABOVE ADDRESS.</p>					
1. REPORT DATE (DD-MM-YY) September 2013		2. REPORT TYPE Conference Paper Preprint		3. DATES COVERED (From - To) 01 October 2011 – 30 September 2013	
4. TITLE AND SUBTITLE ERROR QUANTIFICATION AND CONFIDENCE ASSESSMENT OF AEROTHERMAL MODEL PREDICTIONS FOR HYPERSONIC AIRCRAFT (PREPRINT)				5a. CONTRACT NUMBER In-house	
				5b. GRANT NUMBER	
				5c. PROGRAM ELEMENT NUMBER 61102F	
6. AUTHOR(S) Benjamin P. Smarslok and Adam J. Culler (AFRL/RQHF) Sankaran Mahadevan (Vanderbilt University)				5d. PROJECT NUMBER 3002	
				5e. TASK NUMBER N/A	
				5f. WORK UNIT NUMBER Q184	
7. PERFORMING ORGANIZATION NAME(S) AND ADDRESS(ES) Hypersonic Sciences Branch (AFRL/RQHF) High Speed Systems Division Air Force Research Laboratory, Aerospace Systems Directorate Wright-Patterson Air Force Base, OH 45433-7542 Air Force Materiel Command, United States Air Force			8. PERFORMING ORGANIZATION REPORT NUMBER AFRL-RQ-WP-TP-2013-0273		
9. SPONSORING/MONITORING AGENCY NAME(S) AND ADDRESS(ES) Air Force Research Laboratory Aerospace Systems Directorate Wright-Patterson Air Force Base, OH 45433-7542 Air Force Materiel Command United States Air Force			10. SPONSORING/MONITORING AGENCY ACRONYM(S) AFRL/RQHF		
			11. SPONSORING/MONITORING AGENCY REPORT NUMBER(S) AFRL-RQ-WP-TP-2013-0273		
12. DISTRIBUTION/AVAILABILITY STATEMENT Approved for public release; distribution unlimited.					
13. SUPPLEMENTARY NOTES PA Case Number: 88ABW-2012-1703; Clearance Date: 26 Mar 2012. This paper contains color. The final version of this conference paper was published in the Proceedings of the 53rd AIAA/ASME/ASCE/AHS/ASC Structures, Structural Dynamics, and Materials Conference, held in Honolulu, HI from April 23 through April 26, 2012. The U.S. Government is joint author of the work and has the right to use, modify, reproduce, release, perform, display, or disclose the work.					
14. ABSTRACT Assessing prediction confidence and enabling its use as a decision-making metric for autonomous model fidelity selection is essential to the USAF's vision of a Digital Twin as a viable approach for condition-based fleet management by tail number. Significant strides have been made in modeling complex interactions of the multi-physics, fluid-thermal-structural coupling applicable to hypersonic flow conditions. However, validation of these models remains a challenge due to limited experimental data for hypersonic conditions. This research addresses quantifying errors and assessing the confidence in aerodynamic pressure and heating predictions for a spherical dome protruding from a flat ramp. Well-characterized aerothermal test data from hypersonic wind tunnel experiments are used to calibrate uncertain model parameters and quantify errors through Bayesian techniques. A Bayesian hypothesis testing-based confidence metric is employed to compare the accuracy in various model predictions. A model selection study is performed for 1st-, 2nd-, and 3rd-order piston theories. The results showed that the greatest confidence in model predictions does not necessarily correspond to the highest-order model.					
15. SUBJECT TERMS Bayesian techniques					
16. SECURITY CLASSIFICATION OF:			17. LIMITATION OF ABSTRACT: SAR	18. NUMBER OF PAGES 26	19a. NAME OF RESPONSIBLE PERSON (Monitor) Benjamin P. Smarslok 19b. TELEPHONE NUMBER (Include Area Code) N/A
a. REPORT Unclassified	b. ABSTRACT Unclassified	c. THIS PAGE Unclassified			

Error Quantification and Confidence Assessment of Aerothermal Model Predictions for Hypersonic Aircraft

Benjamin P. Smarslok* and Adam J. Culler†
Air Force Research Laboratory, Wright-Patterson AFB, OH 45433

Sankaran Mahadevan‡
Vanderbilt University, Nashville, TN 37235

Assessing prediction confidence and enabling its use as a decision-making metric for autonomous model fidelity selection is essential to the USAF’s vision of a ‘Digital Twin’ as a viable approach for condition-based fleet management by tail number. Significant strides have been made in modeling complex interactions of the multi-physics, fluid-thermal-structural coupling applicable to hypersonic flow conditions. However, validation of these models remains a challenge due to limited experimental data for hypersonic conditions. This research addresses quantifying errors and assessing the confidence in aerodynamic pressure and heating predictions for a spherical dome protruding from a flat ramp. Well-characterized aerothermal test data from hypersonic wind tunnel experiments are used to calibrate uncertain model parameters and quantify errors through Bayesian techniques. A Bayesian hypothesis testing-based confidence metric is employed to compare the accuracy in various model predictions. A model selection study is performed for 1st-, 2nd-, and 3rd-order piston theories. The results showed that the greatest confidence in model predictions does not necessarily correspond to the highest-order model.

Nomenclature

B	=	Bayes factor
C	=	Bayesian hypothesis testing-based confidence metric
D	=	diameter of the spherical dome
e	=	model error
H	=	height of the spherical dome
M	=	Mach number
p	=	aerodynamic pressure
q	=	dynamic pressure ($\rho U^2/2$)
Q	=	aerodynamic heat flux
R_{eq}	=	equivalence ratio (fuel-to-air ratio divided by stoichiometric fuel-to-air ratio)
S	=	main effect sensitivity index
S_T	=	total effect sensitivity index
T	=	temperature
w	=	transverse panel displacement
x	=	model prediction, location along dome
y	=	observed data
β	=	oblique shock angle relative to freestream
ϕ	=	uncertain input parameters
γ	=	ratio of specific heats
μ	=	mean
π	=	probability density function

*Research Aerospace Engineer, Air Vehicles Directorate, Structural Sciences Center, AIAA Member, benjamin.smarslok@wpafb.af.mil

†Postdoctoral Research Engineer, Universal Technology Corporation, AIAA Member

‡John R. Murray Sr. Chair in Engineering, Civil and Environmental Engineering Department, AIAA Associate Fellow

θ = panel inclination angle to freestream
 ρ = density
 σ = standard deviation

Subscripts

aw = adiabatic wall
e = edge of boundary layer
i = variable index, position along spherical dome
true = true value of x
pred = model prediction of x
w = wall, aerodynamic surface
1 = freestream flow
3 = flow at the leading edge of panel
4 = flow at location of interest along the panel

Superscripts

fp = flat plate
sd = spherical dome
* = flow properties evaluated at Eckert's reference temperature

I. Introduction

ADVANCES in computational capability and model fidelity have inspired the USAF to develop a plan for creating a Digital Twin for every aircraft platform. The Digital Twin vision is to enable condition-based fleet management by tail number through numerical simulation of the structural response to the same flight spectrum as experienced by the physical system. That is, the Digital Twin must be capable of integrating extreme environmental, coupled loading with advanced damage initiation and accumulation models for life prediction. This is especially the case for ultra-high performance platforms, such as reusable, air-breathing hypersonic vehicles, since full-scale testing of the various disciplines is often impractical.¹ Unfortunately, obtaining the needed long time histories from these complex models usually creates an intractable computational problem.² Therefore, it is critical for a hypersonic twin to be capable of autonomously selecting between competing, variable-fidelity models for efficient and accurate representation of coupled fluid-thermal-structural interactions. However, errors inherently exist in all computational model predictions due to imperfect knowledge and physical variability in the system, model order reduction, assumptions and approximations, and the limited experimental data available for model validation. This initial phase of a broader research objective is focused on quantifying the errors in existing aerothermal model predictions^{3,4} corresponding to a set of experiments in a high-temperature wind tunnel.⁵ The methods implemented in this paper will be used as a basis for expanding error quantification and prediction confidence assessments to a coupled aerothermoelastic model.

Aircraft structures exposed to extreme environments are subjected to coupled aerodynamic, thermal, and acoustic loading.^{2,3,6-12} Neglecting these interactions can lead to gross errors in model predictions.¹⁰⁻¹⁵ Aerothermoelastic aircraft structures can be modeled at multiple levels of fidelity for structural and thermal effects. However, there are limitations in computational resources, which make the degree of model fidelity and the level of coupling necessary for a particular problem play a key role in the computational tractability of the model used. For example, aerodynamic pressure and heating could be calculated using a computational fluid dynamics (CFD) model, or the decision could be made to use reduced-order models or the simpler piston theory and Eckert's reference enthalpy method, respectively.^{3,4,12,16} Substantial research has been performed on investigating the model components for the physics of a coupled aerothermoelastic panel and the solution procedures for both quasi-static and dynamic solutions.^{2,3,6-12} However, the current state of the art focuses on deterministic calculations with limited uncertainty analysis. Lamorte et al. investigated the implementation of a stochastic collocation approach for propagating uncertainty in aerothermoelastic analysis.¹⁷ Related work expanded on uncertainty propagation in aerothermoelastic analysis for hypersonic vehicles with emphasis on assessing the impact of aerothermoelastic deformation on aerodynamic heating.¹³ Culler et al. also identified two-way coupling between structural deformation and aerodynamic heating as an important consideration in modeling an aerothermoelastic panel.¹¹ These efforts underscore the importance of understanding the uncertainty in a coupled aerothermoelastic model; however, many questions remain about the significant deterministic and stochastic sources of uncertainty and how to assess the confidence in model predictions.

Obviously, uncertainty is prevalent in any coupled system due to physical variability, sparse data, and modeling errors. Physical variability is inherent in fluid-thermal-structural interactions through variations in material properties, geometry, boundary conditions, and load interactions. Uncertainty also exists in the experimental data used for model calibration and validation due to limited availability and difficulties in creating an experimental environment capable of fully validating the model. This is particularly the case for hypersonic aircraft structures exposed to extreme environments. Finally, the aerothermoelastic model prediction has both model form error and numerical errors. In this context, model form error encompasses the errors in representing the physical system with a particular model. Numerical errors include errors from sampling, discretization, coupled solution procedures, and other mathematical approximations. In the presence of these various uncertainty sources, engineers are challenged with resource allocation, uncertainty quantification, model calibration, and model validation. An attractive option for integrating errors and reducing uncertainty when limited data is available is the use of Bayesian techniques.^{18,19} These techniques provide the statistical information to validate models and quantify the confidence in their predictions. Integrating statistical distributions and observed data in a systematic Bayesian framework for capturing interactions of uncertainty, model predictions, and experimental data is achieved through a Bayes network.^{18,19} A Bayes network is a versatile tool for performing model validation, sensitivity analysis, assessing model extrapolation capability, and determining experimental and computational resource allocation.^{5,18-20} Bayes networks enable the fusion of various forms of information, such as model predictions, experimental data, subjective information, errors, and data uncertainty.²¹

The current research is part of a longer-term initiative to create a framework for integrating various sources of uncertainty in a coupled hypersonic structural simulation and assessing the confidence in model predictions. This study lays the groundwork for the previously discussed Bayes network for a coupled aerothermoelastic system. The four primary objectives of this paper are: 1) perform sensitivity analysis to identify significant variables, 2) calibrate uncertain model inputs and quantify model errors using experimental data with Bayesian updating, 3) validate the predictions using a Bayesian hypothesis testing-based confidence metric, and 4) use the confidence metric to make decisions for model selection. The existing models considered in this study correspond to aerothermal tests performed by NASA on spherical domes protruding from a flat ramp into Mach 6.5 flow.⁵ These comprehensive and unique experiments were conducted in 1986 by Glass and Hunt in the Langley 8-foot High-Temperature Tunnel (HTT)⁵, and the tests are still used for validation purposes in numerous, on-going research efforts.^{3,4}

The outline of the paper is as follows. Section II describes the coupled aerothermoelastic problem, as well as the simplified aerothermal model corresponding to the Glass and Hunt HTT experiments. In Section III, the model error for the aerothermal problem is analyzed in four steps. First, the input uncertainties are defined, along with sensitivity analysis for the aerodynamic pressure and heating calculations. Next, the uncertain model parameters and errors are calibrated using Bayesian updating with data from Glass and Hunt⁵ experiments. Subsequently, the calibrated uncertainty and errors are used for validation with experimental data from a different spherical dome. Finally, a Bayesian hypothesis testing-based confidence metric is used to compare several different model predictions with the experimental data.

II. Aerothermal Model Definition and Experiments

Consider a panel section on the forebody of a representative hypersonic vehicle configuration, as shown in Fig. 1.³ As the vehicle is subjected to hypersonic flow (location '1'), an attached oblique shock is created at the forebody leading edge. This results in aerodynamic pressure at the area of interest (location '4'), causing elastic deformation of the panel, which feeds back to alter the aerodynamic pressure on the panel. This is commonly referred to as the aeroelastic portion of the coupling. The panel is also subjected to aerothermal effects from aerodynamic heating. Naturally, this aerothermal component is coupled to the aeroelastic component, since a change in the temperature of the structure causes additional deformation, which in turn further alters both the aerodynamic pressure and the aerodynamic heating. Figure 2 schematically illustrates these interactions as the coupling of: aerodynamic pressure, aerodynamic heating, heat transfer, and structural deformation.

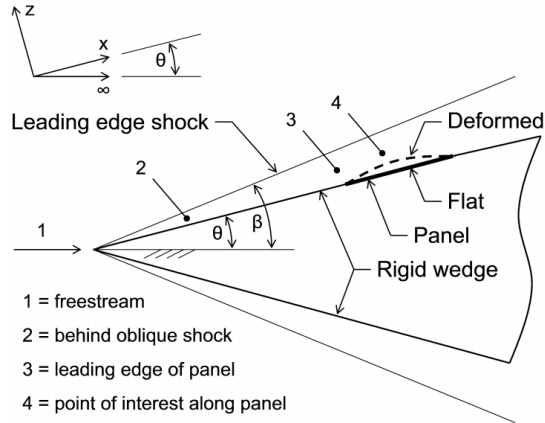


Figure 1. Representative hypersonic vehicle structure with aerothermoelastic panel³

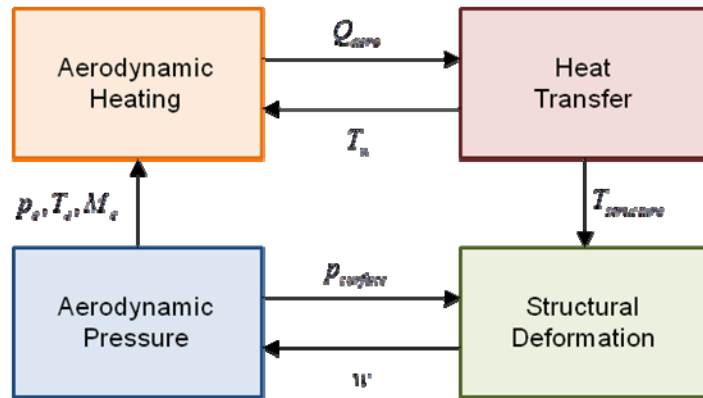


Figure 2. Aerothermoelastic model

Modeling these interactions can be critical for accurately predicting the structural response under hypersonic flow conditions. However, due to the complexity of the problem, presumably less important couplings are typically neglected in favor of a more tractable solution. On-going research is investigating models for each of the four aerothermoelastic system components, as well as their integration to study the importance of different types of coupling.^{3,4,13}

In order to validate these models and quantify the confidence in their predictions, experimental data from this extreme, hypersonic environment is required. A candidate for validation data under these conditions are the experiments performed by Glass and Hunt, in which a series of tests were conducted in a hypersonic wind tunnel to investigate the aerodynamic loads on deformed surface panels.⁵ To simulate a deformed panel, a rigid spherical dome protuberance was mounted on a flat panel holder. While the use of rigid domes removes the aeroelastic coupling, valuable aerothermal data was obtained. The 8-foot High-Temperature Tunnel can simulate up to Mach 7 flow at an altitude between 25 and 40 km for up to 2 minutes by combusting a mixture of methane and air. The flow conditions for the tests of interest had a turbulent boundary-layer at the panel location, and the panel holder had a sharp leading edge, similar to the representative hypersonic vehicle depicted in Fig. 1.

The experiments performed by Glass and Hunt used a flat plate specimen to record the aerodynamic pressure and heat flux at the center of the plate as a reference. In addition, spherical pressure and thermal domes with a diameter of 35.6 cm and the three H/D ratios shown in Table 1 were instrumented. Table 1 also summarizes the freestream conditions p_1 and M_1 , for each test. A schematic of the test specimen and the 58 instrumented locations is shown in Fig. 3. For the purposes of this study, the analysis is limited to the points along the centerline parallel to the flow. An investigation by Ostoich et al.⁴ discovered that the recorded data at points 1 and 38 may have been affected by an uncharacterized gap between the dome and plate, thus only the middle 11 data points along the centerline (points 2 - 39) are considered.

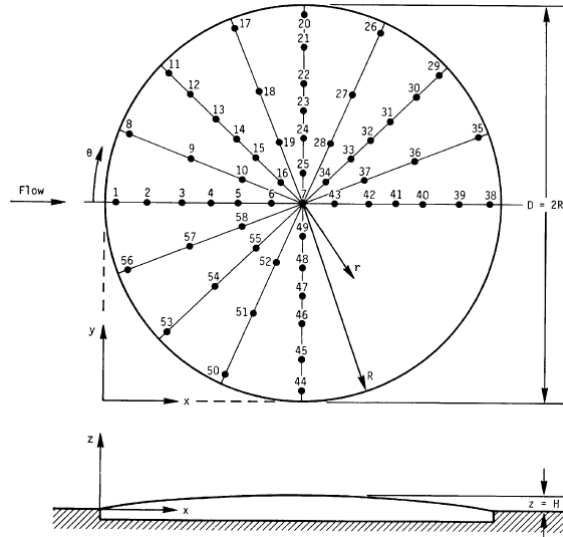


Figure 3. Spherical dome geometry and instrumented locations for HTT measurements⁵

Table 1. Experimental conditions from Glass and Hunt for three tests at different dome heights⁵

Test	p_1	M_1	$(H/D)_{p_4}$	$(H/D)_{Q_4}$
Run 30	654.9	6.60	0.028	0.033
Run 31	648.0	6.60	0.013	0.013
Run 32	645.9	6.60	0.006	0.010

The flat plate and spherical dome measurements provide substantial validation data for error quantification and confidence assessments. Furthermore, since the domes and plate are thick and assumed to be rigid, potential coupling between structural deformation and aerodynamic heating can be neglected. Thus, the aerothermoelastic model in Fig. 2 simplifies to the aerothermal model shown in Fig. 4.

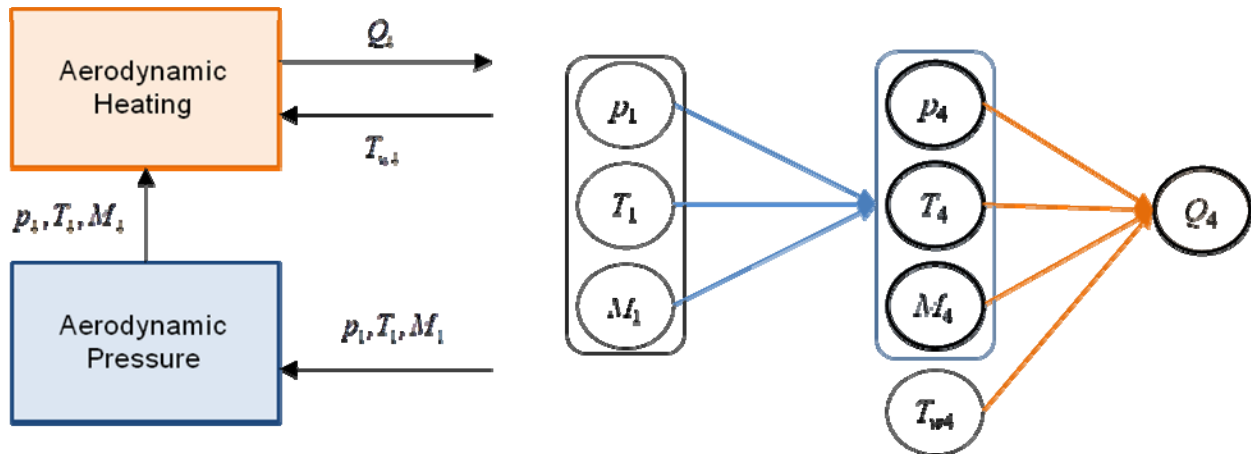


Figure 4. a) Aerodynamic pressure and heating models, b) Propagation of random variables

Figure 4a shows the interaction of the aerodynamic pressure and heating models, and Fig. 4b shows a schematic of uncertainty propagation for the primary random variables. The subscripts of the flow parameters follow the same numbering convention as defined in Fig. 1 for the representative hypersonic vehicle forebody. Location ‘4’ refers to the location(s) of interest on the flat plate (fp) or spherical dome (sd). The oblique shock relations (Eqs. (1)-(4)) give the properties of the inviscid flow (p_3 , T_3 , and M_3) parallel to the inclined surface as a function of the freestream conditions (p_1 , T_1 , and M_1), shock wave angle β , and surface inclination angle θ .²²

$$\frac{p_3}{p_1} = 1 + \frac{2\gamma}{\gamma+1} (M_1^2 \sin^2(\beta) - 1) \quad (1)$$

$$\frac{\rho_3}{\rho_1} = \frac{(\gamma+1)M_1^2 \sin^2(\beta)}{(\gamma-1)M_1^2 \sin^2(\beta) + 2} \quad (2)$$

$$\frac{T_3}{T_1} = \frac{p_3/p_1}{\rho_3/\rho_1} \quad (3)$$

$$M_3^2 \sin^2(\beta - \theta) = \frac{M_1^2 \sin^2(\beta) + \frac{2}{\gamma-1}}{\left(\frac{2}{\gamma-1}\right)M_1^2 \sin^2(\beta) - 1} \quad (4)$$

Equation (1) is used to calculate the aerodynamic pressure prediction on the flat plate, $p_4^{fp} = p_3$. For a deformed surface, or a spherical dome, another model must be used to calculate the aerodynamic pressure, such as piston theory.³ A 3rd-order expansion of piston theory (Eq. (5)) is used in this study, due to the combined presence of hypersonic flow and moderate protrusion of the spherical domes into the flow.

$$p_4^{sd} = p_3 + 2 \frac{q_3}{M_3} \left[\left(\frac{1}{U_3} \frac{\partial w}{\partial t} + \frac{\partial w}{\partial x} \right) + \frac{\gamma+1}{4} M_3 \left(\frac{1}{U_3} \frac{\partial w}{\partial t} + \frac{\partial w}{\partial x} \right)^2 + \frac{\gamma+1}{12} M_3^2 \left(\frac{1}{U_3} \frac{\partial w}{\partial t} + \frac{\partial w}{\partial x} \right)^3 \right] \quad (5)$$

After computing the inviscid flow over the flat plate or spherical dome, the heat flux can be calculated using several different approaches. In a higher-fidelity model, computational fluid dynamics could be employed to predict both the aerodynamic pressure and heating, as done by Ostoich et al.⁴ In the present study, a more computationally expedient method is needed. Eckert's reference temperature method is selected because it provides a rapid approximation for the boundary layer flow, while incorporating local inviscid flow properties (location '4') to capture the first order effect of panel deformation (spherical dome effect in this case). Using flow properties evaluated at Eckert's reference temperature (Eq. (6)) the aerodynamic heat flux is computed using Eq. (7).^{3,23}

$$T^* = T_e + 0.5(T_w - T_e) + 0.22(T_{aw} - T_e) \quad (6)$$

$$Q_4 = St^* \rho^* U_e c_p^* (T_{aw} - T_w) \quad (7)$$

Where, St^* is the reference Stanton number, ρ^* is the reference density, U_e is the inviscid flow velocity, c_p^* is the reference specific heat, T_{aw} and T_w are the adiabatic wall and actual wall temperatures, respectively, and T_e is the boundary layer edge temperature. Note in Eqs. (6) and (7) all flow properties and the wall temperature are evaluated at the point of interest on the flat plate or spherical dome (location '4').

The next section further discusses the uncertain inputs in the aerothermal model, as well as Bayesian model parameter calibration, error quantification, and validation for pressure and heat flux predictions.

III. Investigation of Model Error for Aerothermal Experiments

This section analyzes the prediction error for the Glass and Hunt experiments⁵ using the assumptions and results from Culler et al.³ The use of the Glass and Hunt data in this paper closely follows the aerothermal model verification study performed in Ref. [3]. This work reevaluates some of the assumptions and errors that were observed in the previous study.

First, a description of the uncertain input parameters in the experiments and aerodynamic pressure and heating calculations is provided with sensitivity analysis. Next, two sets of experimental data are used to calibrate uncertain model inputs and errors. The calibrated inputs are then used to update nominal predictions for the spherical dome experiments. Then, a third data set is used for validation with Bayesian hypothesis testing-based confidence. Finally, a model selection study is performed using the confidence metric for different forms of piston theory.

A. Model Input Uncertainty and Sensitivity Analysis

Consider the flat plate specimen, where oblique shock relations are used for aerodynamic pressure p_4^{fp} and Eckert's reference temperature method for aerodynamic heating Q_4^{fp} . Note that for the flat plate, we are interested in the value at the center of the plate, which corresponds to location '4' in Fig. 1. The flat plate experiments consisted of three tests (Runs 30, 31, and 32), which all correspond to the same nominal inputs and turbulent boundary-layer with a sharp leading edge panel holder. For these tests, the freestream pressure p_1 , and Mach number M_1 , were given as shown in Table 1. In addition, the output aerodynamic pressure and heat flux were measured at the center of the flat plate. However, three critical pieces of information were not available in the Glass and Hunt⁵ report: the freestream temperature T_1 , wall temperature T_{w4} , and equivalence ratio R_{eq} . Therefore, realistic values had to be estimated from other reports of similar testing.²⁴ The mean freestream and wall temperatures are assumed to be 220K and 300K, respectively. The equivalence ratio is also uncertain, but for the current investigation a constant value of $R_{eq} = 0.9$ is assumed.

To get a better understanding of the uncertainty in the outputs and their sensitivity to the inputs, statistical distributions were assumed for the inputs. Since p_1 and M_1 were measured, 1% coefficient of variation (CV) is used for measurement variability. However, 10% CV is used for T_1 and T_{w4} since they were not reported and had to be assumed. Normal distributions are used for all four random inputs and their distribution parameters are shown in Table 2.

Table 2. Uncertainty for inputs to aerodynamic pressure and heat flux calculations

Measured Inputs	Mean	Standard Deviation	Coefficient of Variation
p_1 (Pa)	652.5	6.525	1%
M_1	6.6	0.066	1%
Uncertain Inputs	Mean	Standard Deviation	Coefficient of Variation
T_1 (K)	220	22.0	10%
T_{w4} (K)	300	30.0	10%

Local and global sensitivity analyses are performed to investigate the sensitivity of aerodynamic pressure and heating to the input variables. For defining the sensitivity measures, let $Y = f(X_1, X_2, \dots, X_n)$, where X_i is the measured or uncertain inputs and Y is the resulting random output. The local sensitivity is calculated as the difference of the total variance $\text{var}(Y)$, to the variance when each of the corresponding random variables is evaluated at their mean with the other inputs remaining random (Eq. (8)).²¹ The greater the value of $\Delta\sigma_i^2$, the greater the importance of X_i on Y . Note that X_{-i} refers to being calculated over all random variables X_j except X_i . The global sensitivity is expressed as main effect sensitivity index S_i and total effect sensitivity index S_{Ti} shown in Eqs. (9) and (10), respectively.²¹ The S_i of a variable is another measure of the sensitivity of X_i on Y and S_{Ti} provides information about the interaction of X_i with other variables. The sensitivities for the initial random inputs in Table 2 are shown in Table 3.

$$\Delta\sigma_i^2 = \frac{\text{var}(Y) - \text{var}_{X_{-i}}(Y | X_i = \bar{x}_i)}{\text{var}(Y)} \quad (8)$$

$$S_i = \frac{\text{var}_{X_i}[E_{X_{-i}}(Y | X_i)]}{\text{var}(Y)} \quad (9)$$

$$S_{Ti} = \frac{E_{X_{-i}}[\text{var}_{X_i}(Y | X_{-i})]}{\text{var}(Y)} \quad (10)$$

Table 3. Local and global sensitivity for aerodynamic pressure and heat flux for the flat plate with initial uncertainty

Input Variable	$(\Delta\sigma_i^2)^{p_4^{fp}}$	$S_i^{p_4^{fp}}$	$S_{T_i}^{p_4^{fp}}$	$(\Delta\sigma_i^2)^{Q_4^{fp}}$	$S_i^{Q_4^{fp}}$	$S_{T_i}^{Q_4^{fp}}$
p_1 (Pa)	0.686	0.684	0.680	0.020	0.016	0.016
M_1	0.333	0.319	0.319	0.122	0.174	0.175
T_1 (K)	0.0008	0.0002	0.0002	0.451	0.464	0.465
T_{w4} (K)	-	-	-	0.340	0.344	0.344

As expected, the temperatures play a small role in the p_4^{fp} calculation; T_{w4} does not appear in oblique shock relations and T_1 is only used with R_{eq} to determine the methane-air properties. However, T_1 and T_{w4} are dominant in the heat flux calculation with 0.451 and 0.340, respectively. Furthermore, since the sum of the main effect indices S_i is close to 1, individual values of the main effect indices S_i and the total effect indices S_{T_i} are so similar, it is indicated that there is not a strong interaction among variables. Table 4 shows the forward uncertainty propagation of the normal random variables from Table 2 to p_4^{fp} and Q_4^{fp} .

Table 4. Uncertainty propagation using initial uncertainty to pressure and heat flux for the flat plate

Output	Mean	Coefficient of Variation
p_4^{fp} (Pa)	1385.4	1.21%
Q_4^{fp} (W/cm ²)	5.211	11.53%

Observe that the 10% uncertainty in the temperatures (T_1 and T_{w4}) play a larger role in the Q_4^{fp} calculation, therefore it has a larger CV at 11.53%. Since these experimental values are unknown and the distributions are assumed, it is beneficial to calibrate these uncertain model inputs. The next section uses Bayesian updating to calibrate the T_1 and T_{w4} distributions and quantify the model errors using a Bayes network with the Glass and Hunt⁵ data.

B. Bayesian Model Parameter Calibration

There is significant epistemic uncertainty in the true values of T_1 and T_{w4} , therefore Bayesian model parameter calibration can assist in better approximating these values based on observations. Furthermore, the errors in aerodynamic pressure and heat flux for the flat plate and spherical dome predictions can also be calibrated. First, as a brief introduction to Bayesian concepts, let $\boldsymbol{\varphi}$ be the uncertain model parameters or errors in a model $x(\boldsymbol{\varphi})$ with some prior information on the parameters' uncertainty as a basis for a statistical distribution $\pi(\boldsymbol{\varphi})$. Then using some observed data y , the distribution of the unknown parameters is updated using Bayes theorem, as shown in Eq. (11).¹⁸

$$\pi(\boldsymbol{\varphi} | y) = \frac{\Pr[y | x(\boldsymbol{\varphi})] \pi(\boldsymbol{\varphi})}{\int \Pr[y | x(\boldsymbol{\varphi})] \pi(\boldsymbol{\varphi}) d\boldsymbol{\varphi}} \quad (11)$$

Thus, this Bayesian updating reduces the uncertainty in the parameters $\boldsymbol{\varphi}$, given observations y . In this case, the uncertain parameters are $\boldsymbol{\varphi} = [T_1, T_{w4}, e_{p_4}^{fp}, e_{Q_4}^{fp}, e_{p_4}^{sd}, e_{Q_4}^{sd}]$; where, $e_{p_4}^{fp}$, $e_{Q_4}^{fp}$, $e_{p_4}^{sd}$, and $e_{Q_4}^{sd}$ are the errors in the aerodynamic pressure and heat flux predictions for the flat plate and spherical dome specimens. The model error is defined as the difference between the model prediction and the true value, as shown in Eqs. (12) and (13) for the flat plate and spherical dome models, respectively. For this study, a systematic error in the predictions across the dome is assumed for convenience, as seen in Eq. (13).

$$p_{4_{true}}^{fp} = p_{4_{pred}}^{fp} + e_{p_4}^{fp} \quad Q_{4_{true}}^{fp} = Q_{4_{pred}}^{fp} + e_{Q_4}^{fp} \quad (12)$$

$$\left(p_{4_{true}}^{sd} \right)_i = \left(p_{4_{pred}}^{sd} \right)_i + e_{p_4}^{sd} \quad \left(Q_{4_{true}}^{sd} \right)_i = \left(Q_{4_{pred}}^{sd} \right)_i + e_{Q_4}^{sd} \quad (13)$$

Building upon the relationship of the inputs and predictions from Fig. 4b, a Bayes network of the measured inputs (p_1 and M_1), uncertain inputs (T_1 and T_{w4}), model predictions (p_4 and Q_4), and model errors (e_{p_4} and e_{Q_4}) is constructed. Figure 5 depicts the Bayes network for the aerodynamic pressure and heat flux predictions for the flat plate and spherical dome geometries and the interconnections between inputs, errors, and data.

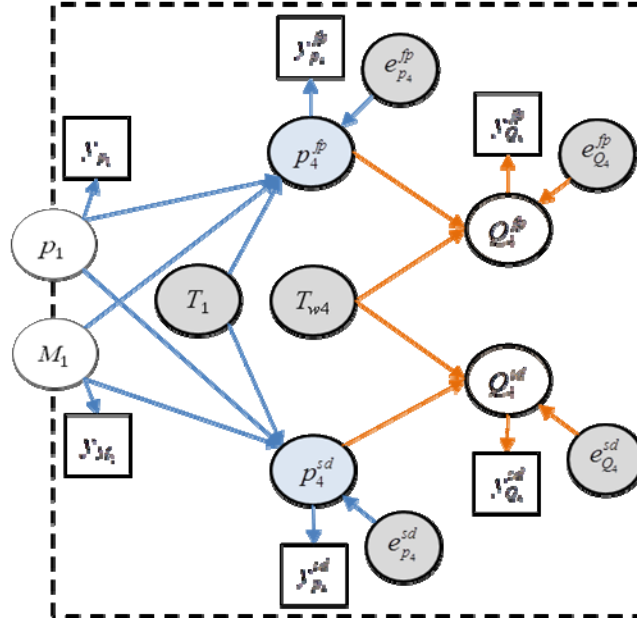


Figure 5. Bayes network for calibrating model inputs and errors using Glass and Hunt data⁵

The gray nodes in Fig.5 are the uncertain inputs and errors that are being calibrated with the Glass and Hunt⁵ data. The dashed-box around the network represents the randomness in the measured inputs p_1 and M_1 . Bayes theorem in Eq. (11) is rewritten for the case corresponding to the aerodynamic pressure and heat flux predictions for the Glass and Hunt⁵ experiments in Eq. (14).

$$\pi(\boldsymbol{\varphi} | y_{p_4}, y_{Q_4}, y_{p_1}, y_{M_1}) = \frac{\Pr[y_{p_4}, y_{Q_4}, y_{p_1}, y_{M_1} | P_4(\boldsymbol{\varphi}), Q_4(\boldsymbol{\varphi}), p_1, M_1] \pi(\boldsymbol{\varphi})}{\int \Pr[y_{p_4}, y_{Q_4}, y_{p_1}, y_{M_1} | P_4(\boldsymbol{\varphi}), Q_4(\boldsymbol{\varphi}), p_1, M_1] \pi(\boldsymbol{\varphi}) d\boldsymbol{\varphi}} \quad (14)$$

In Eq. (14), uncertain inputs and errors are $\boldsymbol{\varphi} = [T_1, T_{w4}, e_{p_4}^{fp}, e_{Q_4}^{fp}, e_{p_4}^{sd}, e_{Q_4}^{sd}]$, data is available for y_{p_4} and y_{Q_4} from the flat plate and spherical dome measurements, as well as measured input data y_{p_1} and y_{M_1} (Table 1). Therefore, all four sources of data are incorporated in the likelihood function. Now that $\boldsymbol{\varphi}$ and y are identified, we must now define the prior distributions $\pi(\boldsymbol{\varphi})$. Normal distributions are used for uncertain inputs T_1 and T_{w4} , with means from Culler et al.³ and 10% coefficient of variation, as summarized in Table 2. Regarding model errors, observations from previous reports indicated that p_4 and Q_4 predictions are expected to be accurate within [-10%, +10%] and [-10%, -30%], respectively.²⁴ The error bounds for Q_4 are associated with Eckert's reference temperature method, which is expected to consistently over-predict the true value due to the calorically perfect gas assumption. However, after a preliminary comparison of predictions to data, a uniform distribution over the range [-30%, +30%] of the

prediction was determined to be a more appropriate prior for all four error terms in this study. Therefore, this error model assumes uniform distributions based on the experimental means for the prior distribution of errors $\pi(\boldsymbol{\varphi})$. Normal distributions are used for the likelihood function $\Pr[y|x(\boldsymbol{\varphi})]$, where the distribution parameters from Table 2 are assumed for y_{p_1} and y_{M_1} , whereas 5% measurement uncertainty is assumed for aerodynamic pressure and heat flux measurements y_{p_4} and y_{Q_4} .

Bayesian updating according to Eq. (14) is performed using all of the observed data from Glass and Hunt⁵, except for Run 30 for the spherical dome. Run 30 data is reserved for validation, which is discussed in the following section. When performing the Bayesian updating, the freestream pressure p_1 , and Mach number M_1 , are also treated stochastically due to the measurement uncertainty presented in Table 2 with 1% CV. Equation (14) is evaluated at 100 realizations of p_1 and M_1 using Latin Hypercube sampling. For each of those samples, a Markov Chain Monte Carlo (MCMC) algorithm called slice sampling is employed using 10^4 samples to calculate the posterior distribution. Figures 6 and 7 show the integrated posterior distributions for the uncertain inputs and errors $\boldsymbol{\varphi} = [T_1, T_{w4}, e_{p_4}^{fp}, e_{Q_4}^{fp}, e_{p_4}^{sd}, e_{Q_4}^{sd}]$.

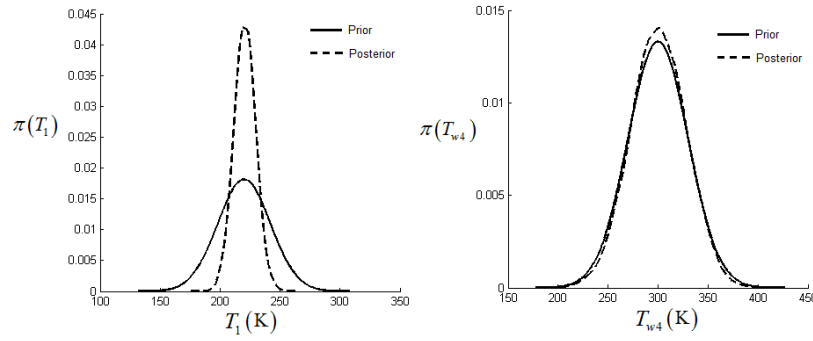


Figure 6. Prior and posterior distributions for a) freestream temperature T_1 , and b) wall temperature T_{w4}

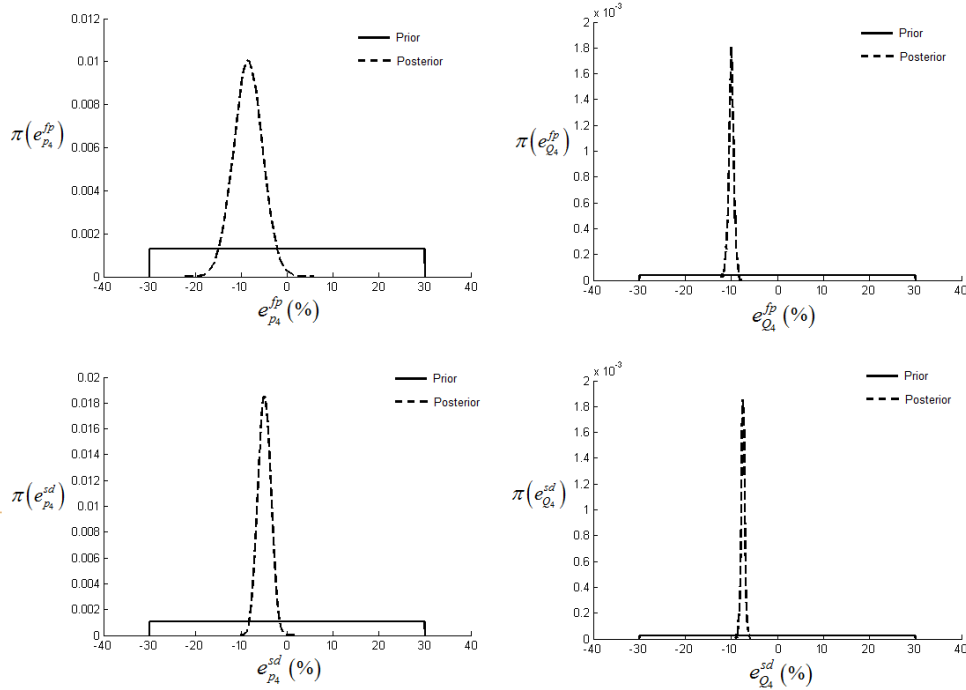


Figure 7. Prior and posterior distributions for a) error in flat plate p_4 , b) error in flat plate Q_4 , c) error in spherical dome p_4 , and d) error in spherical dome Q_4

The mean and standard deviation of the posterior distributions for $\boldsymbol{\varphi} = [T_1, T_{w4}, e_{p_4}^{fp}, e_{Q_4}^{fp}, e_{p_4}^{sd}, e_{Q_4}^{sd}]$ are shown in Table 5. Comparing the initial and updated distributions of T_1 and T_{w4} , it is seen that the uncertainty is reduced, however the mean value did not shift. This is primarily a result of the errors in p_4 and Q_4 predictions being more easily scaled as defined in Eqs. (12) and (13). Thus, calibrating the errors did result in a shift in the mean values, as seen in Fig. 7. Also, there is significant uncertainty reduction in the errors from the initial $\pm 30\%$.

Table 5. Mean, standard deviation, and coefficient of variation of calibrated model inputs and errors

Output	Mean	Standard Deviation	Coefficient of Variation
T_1 (K)	220.67	9.25	4.19%
T_{w4} (K)	300.34	28.24	9.40%
$e_{p_4}^{fp}$ (Pa)	-108.87 (-8.5%)	40.36	37.07%
$e_{Q_4}^{fp}$ (W/cm^2)	-4707.0 (-10.0%)	280.2	5.95%
$e_{p_4}^{sd}$ (Pa)	-75.84 (-5.0%)	21.28	28.06%
$e_{Q_4}^{sd}$ (W/cm^2)	-4682.6 (-7.5%)	247.8	5.29%

The calibrated distributions for T_1 and T_{w4} are propagated to p_4^{fp} and Q_4^{fp} in Table 6. The uncertainty in aerodynamic pressure is unchanged since it is insensitive to freestream temperature. However, the uncertainty in Q_4^{fp} is reduced from 11.53% to 6.46%.

Table 6. Uncertainty propagation using updated uncertainty to pressure and heat flux for the flat plate

Output	Mean	Coefficient of Variation
p_4^{fp} (Pa)	1385.4	1.23%
Q_4^{fp} (W/cm^2)	5.229	6.46%

The next section investigates the effect of quantifying the model errors in the predictions for the spherical dome and uses the remaining set of data (Run 30) for assessing the confidence in p_4^{sd} and Q_4^{sd} predictions.

C. Assessing Prediction Confidence for Model Validation

The aerodynamic pressure and heat flux along the spherical dome is evaluated at the initial and updated values of $\boldsymbol{\varphi} = [T_1, T_{w4}, e_{p_4}^{sd}, e_{Q_4}^{sd}]$ from Table 5. Figures 8 and 9 show the experimental data from Glass and Hunt⁵ (Runs 30, 31, and 32), along with the initial and updated model predictions p_4^{sd} and Q_4^{sd} evaluated at the mean along the streamwise centerline of the spherical domes (see Fig. 3). Tables 7 and 8 summarize the deterministic errors in the predictions. As illustrated in Figs. 8 and 9, aerodynamic pressure and heating are greatest near the leading edge of the dome and lowest near the trailing edge. This is a result of the slope of the dome in the flow direction, where positive slope results in elevated values and negative slope produces lower values relative to the flat plate. Thus, the largest dome (Run 30) produces the greatest spatial variations in pressure and heating. Note that the slope of each dome is zero at $x/D=0.5$. At this location, pressure and heating values are nearly identical for each dome and for the flat plate, which indicates that local surface inclination has a strong impact on local pressure and heating values.

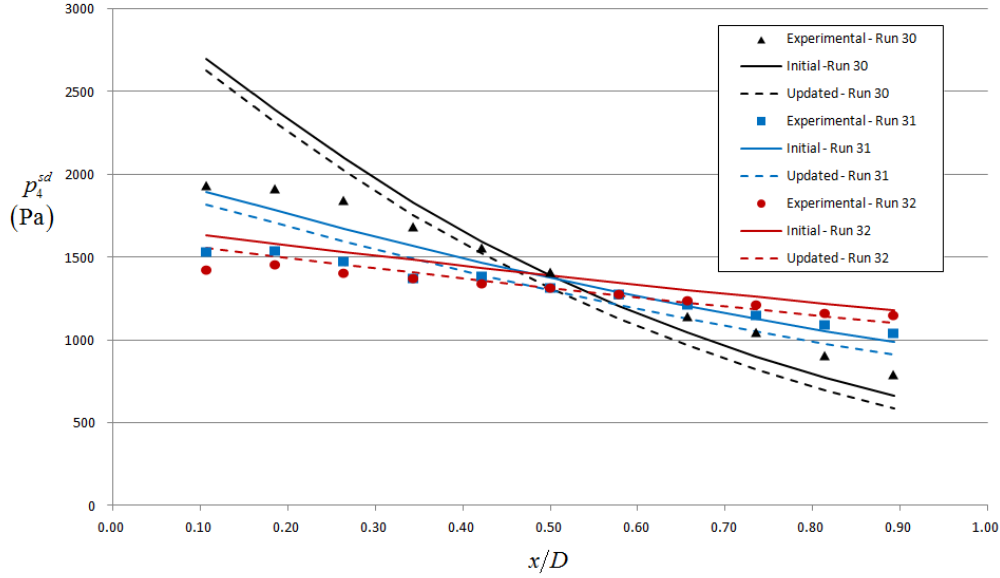


Figure 8. Aerodynamic pressure along centerline of spherical dome for Runs 30, 31, and 32 from experimental data, initial mean input values, and Bayesian updated mean input values

Table 7. Error summary for nominal pressure predictions along centerline of spherical dome

	Initial Errors in p_4^{sd}			Updated Errors in p_4^{sd}		
	Run 30	Run 31	Run 32	Run 30	Run 31	Run 32
Average	13.6%	8.2%	6.7%	16.0%	8.3%	2.7%
Maximum	39.3%	23.5%	14.2%	35.4%	18.5%	8.9%

From Fig. 8 and Table 7 it is evident that 3rd-order piston theory predictions of p_4^{sd} become less accurate with increasing dome surface inclination. Accordingly, the largest error in p_4^{sd} occurs at the forward-most location in Run 30. Recall that Run 30 was saved for validation and only Runs 31 and 32 were included in calibration. This generally resulted in smaller errors for Runs 31 and 32, but errors for Run 30 increased, as summarized in Table 7. It is expected that if data from Run 30 had been included in calibration, then the corresponding errors would have also been reduced. Furthermore, since the errors in p_4^{sd} along the dome vary in magnitude spatially, it would be beneficial to use a more flexible error model, such as a Gaussian process model, in more practical applications.²⁶

Figure 9 and Table 8 show that Eckert's reference temperature method predicted Q_4^{sd} more accurately than 3rd-order piston theory predicted p_4^{sd} . Again, the trend is observed that errors are reduced using the updated ϕ values for Runs 31 and 32, but not Run 30. This may be expected since values of $y_{Q_4}^{sd}$ from Runs 31 and 32 are included in the Bayesian calibration, whereas values from Run 30 were not used.

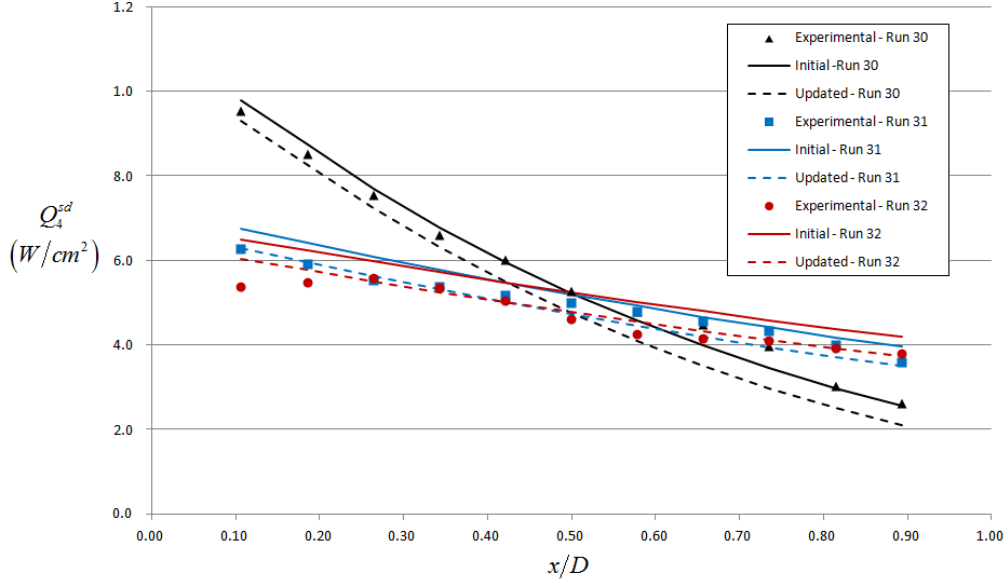


Figure 9. Aerodynamic heat flux along centerline of spherical dome for Runs 30, 31, and 32 from experimental data, initial mean input values, and Bayesian updated mean input values

Table 8. Error summary for nominal heat flux predictions along centerline of spherical dome

	Initial Errors - Q_4^{sd}			Updated Errors - Q_4^{sd}		
	Run 30	Run 31	Run 32	Run 30	Run 31	Run 32
Average	3.9%	6.2%	12.8%	11.7%	4.1%	3.6%
Maximum	12.9%	10.4%	21.2%	24.7%	8.7%	12.4%

The deterministic errors are useful for assessing the accuracy of the nominal model predictions, however this is a stochastic problem and error alone does not provide a statistical assessment of the confidence in the model prediction. Therefore, the most important step in this model uncertainty framework is to validate the models by assessing the confidence. This enables decision-making in regard to model development and fidelity selection. For the Aircraft Digital Twin, it is important to have this confidence metric to make autonomous decision making possible for efficient simulations and risk mitigation.

Several validation metrics exist with advantages and disadvantages, such as classical hypothesis testing, and difference and area metrics; however Bayesian hypothesis testing is selected for this study.^{18,27,28} The Bayes factor approach fits appropriately with the Bayes network integration framework, but its main advantages are that it takes into account the entire probability distribution of the model output and its relation to a confidence metric is straightforward. For Bayesian hypothesis testing, we want to determine the probability of our model being correct, given some observed data. Consider a hypothesis test to determine the probability that a model prediction x is equal to its true value x_0 . Equation (15) calculates the Bayes factor B , as the ratio of likelihoods corresponding to the null hypothesis (model prediction is equal to the true value) and the alternate hypothesis (model prediction is not equal to the true value). Therefore, when $B > 1$, the data supports the null hypothesis better than the alternative hypothesis. The integral form of the Bayes factor in Eq. (15) includes the likelihood function of the data supporting the prediction $\Pr(y|x)$, the probability density function (PDF) of the model prediction $\pi_0(x)$, and the PDF for the alternative hypothesis $\pi_1(x)$.

$$B(x_0) = \frac{\Pr(y|H_0 : x = x_0)}{\Pr(y|H_1 : x \neq x_0)} = \frac{\int \Pr(y|x) \pi_0(x) dx}{\int \Pr(y|x) \pi_1(x) dx} \quad (15)$$

Equation (15) is rewritten in Eqs. (16) and (17) for the cases for aerodynamic pressure and heat flux, where $i = 1$ to 11 for the x -location across the dome.

$$B(p_{4_{0i}}^{sd}) = \frac{\int \Pr(y_{p_{4i}^{sd}} | p_{4i}^{sd}) \pi_0(p_{4i}^{sd}) dp_{4i}^{sd}}{\int \Pr(y_{p_{4i}^{sd}} | p_{4i}^{sd}) \pi_1(p_{4i}^{sd}) dp_{4i}^{sd}} \quad (16)$$

$$B(Q_{4_{0i}}^{sd}) = \frac{\int \Pr(y_{Q_{4i}^{sd}} | Q_{4i}^{sd}) \pi_0(Q_{4i}^{sd}) dQ_{4i}^{sd}}{\int \Pr(y_{Q_{4i}^{sd}} | Q_{4i}^{sd}) \pi_1(Q_{4i}^{sd}) dQ_{4i}^{sd}} \quad (17)$$

The Bayes factor is calculated at each of the 11 points along the spherical dome used in Run 30 of the Glass and Hunt⁵ study. The likelihood function $\Pr(y|x)$ is based on the assumption of a normal distribution for measurement error, with a standard deviation based on 5% coefficient of variation on the mean of the pressure and heat flux data for Run 30 ($N(y_i, 0.05\bar{y})$). The probability density function for the null hypothesis $\pi_0(x)$, is determined by propagating the uncertainty in p_1 , M_1 , T_1 , and T_{w4} , as well as the quantified errors for the spherical dome ($e_{p_4}^{sd}$ and $e_{Q_4}^{sd}$). The PDF for the alternative hypothesis $\pi_1(x)$, is modeled as a uniform distribution extending beyond the maximum and minimum values of p_4^{sd} and Q_4^{sd} predictions.

The Bayes factors computed in Eqs. (16) and (17) can be used to the confidence C , in the prediction, as shown in Eq. (18).²⁵

$$C = \frac{B}{B+1} = P(H_0 | y) \quad (18)$$

As indicated in Eq. (18), C is simply the posterior probability of the null hypothesis being true, given the observation data (under the assumption that prior probabilities of the null and alternative hypotheses are both 0.5). For a Bayes factor of 1.0, the confidence C , is equal to 50%. This implies that we do not have enough evidence to reject or accept the null hypothesis. However, for Bayes factors greater than 1.0 (as explained for Eq. (15)), we would have increasing confidence that the prediction is equal to the true value. The confidence metric can be used as a resource allocation measure for determining when it is beneficial to perform tests, where higher fidelity models are required, and which disciplines need a more strongly (or less strongly) coupled solution procedure. In addition, the Bayes factor-based confidence can be used to assess the limits of the model's predictions.

Table 9 summarizes the confidence (Eqs. (16)-(18)) and deterministic error in p_4^{sd} and Q_4^{sd} predictions for the 11 observations from Run 30 ($y_{p_{4i}^{sd}}$ and $y_{Q_{4i}^{sd}}$).

Table 9. Error and confidence in aerodynamic pressure and heat flux predictions along centerline of spherical dome for Run 30

Location	x/D	%error p_4^{sd}	$C_{p_{4i}^{sd}}$	%error Q_4^{sd}	$C_{Q_{4i}^{sd}}$
1	0.11	-35.4%	0.00%	2.5%	86.7%
2	0.19	-21.0%	0.02%	2.8%	87.5%
3	0.26	-9.3%	71.1%	3.9%	87.7%
4	0.34	-3.9%	94.0%	4.4%	88.6%
5	0.42	2.4%	94.6%	8.4%	85.1%
6	0.50	7.0%	88.7%	9.7%	85.0%
7	0.58	11.3%	74.8%	14.5%	74.1%
8	0.66	15.3%	54.9%	21.3%	36.1%
9	0.74	21.4%	16.4%	24.7%	25.0%
10	0.81	23.7%	21.7%	17.1%	81.8%
11	0.89	25.9%	30.2%	19.7%	81.5%

The majority of the predictions have greater than 50% confidence, which means the data supports the prediction. Pressure predictions at locations 4-6 have the highest confidence. The confidence in Q_4^{sd} predictions using Eckert's reference temperature method are all above 80%, with the exception of locations 7-9. As mentioned for Fig. 8, the largest error in the p_4^{sd} occurs at the front of the dome, which corresponds to 0% confidence. The deterministic errors give an indication of the quality of the nominal predictions, however note that it is not always indicative of the statistical confidence in the predicted values. For example, 2.4% error at location 5 for p_4^{sd} corresponds to 94.6% confidence, but 2.5% error at location 1 for Q_4^{sd} is lower at 86.7% confidence. This is the result of differences in the shape of the model error distributions for p_4^{sd} and Q_4^{sd} .

The scope of this work is to initiate a framework for assessing the confidence in coupled aerothermoelastic model predictions, not to necessarily draw definitive conclusions for these particular aerodynamic models. However, given the confidence associated with the p_4^{sd} predictions for Run 30 ($H/D = 0.028$), one would likely conclude that 3rd-order piston theory is inadequate for predicting the aerodynamic pressure on a spherical dome protuberance of this size. Although, to truly reach that conclusion, more thorough uncertainty quantification is required to better capture the model error.

The final section builds upon the conclusions using the Bayes factor-based confidence and uses that metric to compare predictions using different forms of piston theory.

D. Model Selection from Prediction Confidence Metric

The Bayes factor-based confidence metric is also useful for model selection. Up to this point, a 3rd-order expansion of piston theory from Eq. (5) was used to predict p_4^{sd} . Naturally, 1st- and 2nd-order expansions could have been used instead. Consider 1st- and 2nd-order piston theories for a model selection study, as shown in Eqs. (19) and (20), respectively.

$$p_4^{sd} = p_3 + 2 \frac{q_3}{M_3} \left(\frac{1}{U_3} \frac{\partial w}{\partial t} + \frac{\partial w}{\partial x} \right) \quad (19)$$

$$p_4^{sd} = p_3 + 2 \frac{q_3}{M_3} \left[\left(\frac{1}{U_3} \frac{\partial w}{\partial t} + \frac{\partial w}{\partial x} \right) + \frac{\gamma+1}{4} M_3 \left(\frac{1}{U_3} \frac{\partial w}{\partial t} + \frac{\partial w}{\partial x} \right)^2 \right] \quad (20)$$

Figures 10 and 11 show the p_4^{sd} and Q_4^{sd} predictions for Run 30 using 1st-, 2nd-, and 3rd-order piston theories. Recall that Eckert's reference temperature method uses the p_4^{sd} predictions from piston theory, so Q_4^{sd} is also affected.

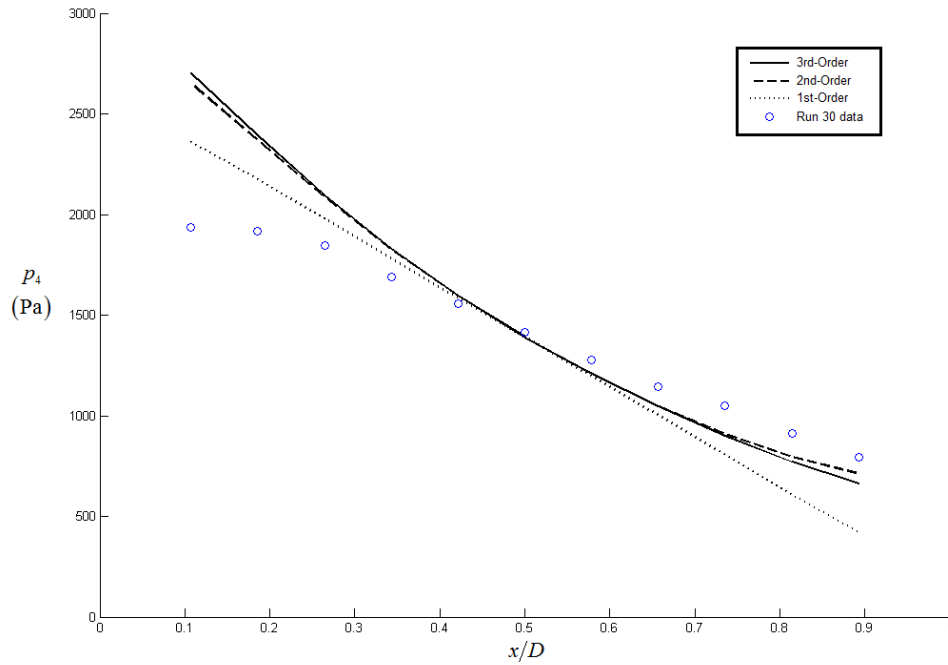


Figure 10. Aerodynamic pressure predictions for Run 30 using 1st-, 2nd-, and 3rd-order piston theory

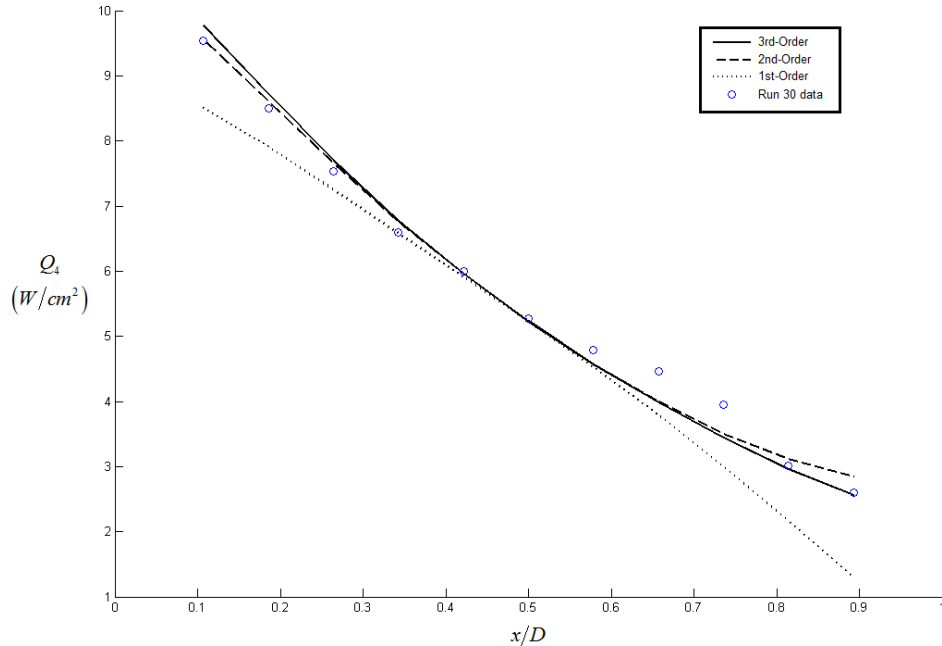


Figure 11. Aerodynamic heat flux predictions for Run 30 using 1st-, 2nd-, and 3rd-order piston theory

Comparing the different piston theories, both 2nd- and 3rd-order capture some of the nonlinearity in p_4^{sd} and Q_4^{sd} and give relatively similar predictions. First-order piston theory appears to give a more accurate prediction at the

front of the dome for p_4^{sd} , however the aft portion has larger errors than 2nd- and 3rd-order. Furthermore, the 1st-order expansion decreases the overall accuracy over the entire dome for heat flux predictions.

Table 10 shows the Bayesian hypothesis testing-based confidence metric for p_4^{sd} and Q_4^{sd} using 1st-, 2nd-, and 3rd-order piston theory. As expected from Fig. 10, 1st-order piston theory has higher confidence at the front of the pressure dome, but is significantly lower when compared to 2nd- and 3rd-order predictions along the centerline of the dome. When comparing the confidence in 2nd- and 3rd-order p_4^{sd} and Q_4^{sd} , not only are the two predictions very similar, but the confidence in the 2nd-order model is actually higher at locations 8-11. Therefore, not only would a lower-order model theoretically require lower computational costs, but it is statistically more representative of observations along the dome for Run 30.

Table 10. Confidence in aerodynamic pressure and heat flux predictions using 1st-, 2nd-, and 3rd-order piston theory along centerline of spherical dome for Run 30

Location	x/D	$C_{p_4^{sd}}$			$C_{Q_4^{sd}}$		
		1 st -order	2 nd -order	3 rd -order	1 st -order	2 nd -order	3 rd -order
1	0.11	0.36%	0.00%	0.00%	31.5%	84.8%	86.7%
2	0.19	63.1%	0.09%	0.02%	62.2%	86.7%	87.5%
3	0.26	94.4%	75.6%	71.1%	77.8%	87.5%	87.7%
4	0.34	95.4%	94.0%	94.0%	85.7%	88.5%	88.6%
5	0.42	94.2%	94.7%	94.6%	83.8%	85.2%	85.1%
6	0.50	89.0%	89.1%	88.7%	84.7%	85.0%	85.0%
7	0.58	68.6%	74.9%	74.8%	69.3%	73.8%	74.1%
8	0.66	20.3%	57.1%	54.9%	10.6%	38.3%	36.1%
9	0.74	0.16%	23.3%	16.4%	0.25%	35.0%	25.0%
10	0.81	0.00%	42.7%	21.7%	0.23%	88.8%	81.8%
11	0.89	0.00%	69.0%	30.2%	0.00%	92.0%	81.5%

IV. Summary

A framework to quantify the model error and assess the confidence in model predictions for a coupled aerothermoelastic panel is outlined. Bayesian model calibration, error quantification, and prediction confidence assessment procedures are described for aerothermal models with data available from tests performed in a High-Temperature Tunnel on spherical dome protuberances subjected to hypersonic flow. The models include 3rd-order expansion of piston theory and Eckert's reference temperature method to predict aerodynamic pressure and heat flux, respectively. This research aims to logically and optimally use the limited data available for model validation and decision-making. The freestream and wall temperatures are assumed since their values were not reported in the experiments. Bayesian calibration is employed to update the uncertain inputs and quantify errors associated with aerodynamic pressure and heat flux predictions. The calibrated input distributions and quantified model errors are used to update the model predictions along the centerline of a spherical dome specimen. The information on the model error is used to calculate the Bayesian hypothesis testing-based confidence to enable model validation and model selection for this aerothermal problem. For this model selection study among piston theories, it was observed that the highest-order model (3rd-order) did not result in the highest prediction confidence metric. The capability to have a metric for autonomously making decisions on aerothermoelastic model fidelity is critical for the USAF Digital Twin vision, and this study is aimed at taking steps to achieve this goal.

V. Acknowledgments

This research is sponsored by the Air Force Office of Scientific Research (AFOSR). The authors gratefully acknowledge the support of AFOSR program managers Drs. Fariba Fahroo and David Stargel. This document has been approved for public release as case number 88ABW-2012-1703 on 26 March 2012.

References

- ¹Dugundji, J., and Calligeros, J. M., "Similarity Laws for Aerothermoelastic Testing," *Journal of the Aero/Space Sciences*, Vol. 29, No. 8, 1962, pp. 935-950.
- ²McNamara, J.J. and Friedmann, P.P., "Aeroelastic and Aerothermoelastic Analysis of Hypersonic Vehicles: Past, Present, and Future," *AIAA Journal*, Vol. 49, No. 6, June 2011, pp. 1089-1122.
- ³Culler, A.J. and McNamara, J.J., "Studies on Fluid-Thermal-Structural Coupling for Aerothermoelasticity in Hypersonic Flow," *AIAA Journal*, Vol. 48, No. 8, 2010, pp. 1721-1738.
- ⁴Ostoich, C., Bodony, D.J., and Geubelle, P.H., "Development and Validation of a First Principles Fluid-Thermal Multi-Physics Solver for Hypersonic Boundary Layer Heat Transfer Problems," *Proc., 52nd AIAA/ASME/ASCE/AHS/ASC Structures, Structural Dynamics & Materials Conf.*, AIAA 2011-1964, Denver, CO, 2011.
- ⁵Glass, C.E. and Hunt, L.R., "Aerothermal Tests of Spherical Dome Protuberances on a Flat Plate at a Mach Number of 6.5," NASA TP-2631, 1986.
- ⁶Thornton, E. A. and Dechaumphai, P., "Coupled Flow, Thermal, and Structural Analysis of Aerodynamically Heated Panels," *AIAA Journal*, Vol. 25, No. 11, 1988, pp. 1052-1059.
- ⁷Kontinos, D., "Coupled Thermal Analysis Method with Application to Metallic Thermal Protection Panels," *Journal of Thermophysics and Heat Transfer*, Vol. 11, No. 2, 1997, pp. 173-181.
- ⁸Blevins, R.D., Bofilios, D., Holehouse, I., Hwa, V.W., Tratt, M.D., Laganelli, A. L., Pozefsky, P., and Pierucci, M., "Thermo-Vibro-Acoustic Loads and Fatigue of Hypersonic Flight Vehicle Structure - Phase II Report." Rohr Industries, Inc., RHR 89-202, November 1989; or, AFRL Technical Report: AFRL-RB-WP-TR-2009-3139, June 2009.
- ⁹Blevins, R. D., Holehouse, I., and Wentz, K.R., "Thermoacoustic Loads and Fatigue of Hypersonic Vehicle Skin Panels," *Journal of Aircraft*, Vol. 30, No. 6, 1993, pp. 971-978.
- ¹⁰Culler, A.J. and McNamara, J.J., "Impact of Fluid-Thermal-Structural Coupling on Response Prediction of Hypersonic Skin Panels," *AIAA Journal*, Vol. 49, No. 11, November 2011, pp. 2393-2406.
- ¹¹Culler, A.J. and McNamara, J.J., "Fluid-Thermal-Structural Modeling and Analysis of Hypersonic Structures under Combined Loading," *52nd AIAA/ASME/ASCE/AHS/ASC Structures, Structural Dynamics & Materials Conference*, AIAA 2011-1965, Denver, CO, 2011.
- ¹²Falkiewicz, N.J. and Cesnik, C.E.S., "Enhanced Modal Solutions for Structural Dynamics in Aerothermoelastic Analysis," *52nd AIAA/ASME/ASCE/AHS/ASC Structures, Structural Dynamics & Materials Conference*, AIAA 2011-1963, Denver, CO, 2011.
- ¹³Lamorte, N., Friedmann, P.P., Dalle, D.J., Torrez, S.M., and Driscoll, J.F., "Uncertainty Propagation in Integrated Airframe-P propulsion System Analysis for Hypersonic Vehicles," *17th AIAA International Space Planes and Hypersonic Systems and Technologies Conference*, AIAA 2011-2394, San Francisco, CA, 2011.
- ¹⁴Weiting, A.R., Dechaumphai, P., Bey, K., Thornton, E.A., and Morgan, K., "Application of Integrated Fluid-Thermal-Structure Analysis Methods," NASA TM-100625, 1988.
- ¹⁵Pettit, C., "Uncertainty Quantification in Aeroelasticity: Recent Results and Research Challenges," *Journal of Aircraft*, Vol. 41, No. 5, 2008, pp. 1217-1229.
- ¹⁶Crowell, A.R., McNamara, J.J., and Miller, B.A., "Surrogate Based Reduced-Order Aerothermodynamic Modeling for Structural Response Prediction at High Mach Numbers," *52nd AIAA/ASME/ASCE/AHS/ASC Structures, Structural Dynamics & Materials Conference*, AIAA 2011-2014, Denver, CO, 2011.
- ¹⁷Lamorte, N., Glaz, B., Friedmann, P.P., Culler, A.J., Crowell, A.R., and McNamara, J.J., "Uncertainty Propagation in Hypersonic Aerothermoelastic Analysis," *51st AIAA/ASME/ASCE/AHS/ASC Structures, Structural Dynamics & Materials Conference*, AIAA 2010-2964, Orlando, FL, 2010.
- ¹⁸Rebba, R. and Mahadevan, S., "Model Predictive Capability Assessment under Uncertainty," *AIAA Journal*, Vol. 44, No. 10, 2006, pp. 2376-2384.
- ¹⁹Normand, S.L. and Tritchler, D., "Parameter Updating in Bayes Network," *Journal of the American Statistical Association*, Vol. 87, No. 420, 1992, pp. 1109-1115.
- ²⁰Shankararaman, S., McLemore, K., Liang, C., Mahadevan, S., Bradford, S.C., and Peterson, L., "Test Resource Allocation for Uncertainty Quantification of Multi-Level and Coupled Systems," *52nd AIAA/ASME/ASCE/AHS/ASC Structures, Structural Dynamics & Materials Conference*, AIAA 2011-1964, Denver, CO, 2011.
- ²¹Liang, B. and Mahadevan, S., "Error and Uncertainty Quantification and Sensitivity Analysis in Mechanics Computational Models," *International Journal for Uncertainty Quantification*, Vol. 1, No. 2, 2011, pp. 147-161.
- ²²Anderson, Jr., J. D., *Modern Compressible Flow with Historical Perspective*, McGraw-Hill, New York, 3rd ed., 2003.
- ²³Eckert, E.R.G., "Engineering Relations for Heat Transfer and Friction in High-Velocity Laminar and Turbulent Boundary-Layer Flow over Surfaces with Constant Pressure and Temperature," *Transactions of the ASME*, Vol. 78, No. 6, 1956, pp. 1273-1283.
- ²⁴Deveikis, W.D. and Hunt, L.R., "Loading and Heating of a Large Flat Plate at Mach 7 in the Langley 8-Foot High-Temperature Structures Tunnel," NASA TN D-7275, September 1973.
- ²⁵Rebba, R. Mahadevan, S., and Huang, S., "Validation and Error Estimation of Computational Models," *Reliability Engineering and System Safety*, Vol. 91, 2006, pp. 1390-1397.

²⁶ Rangavajhala, S., Sura, V.S., Hombal, V.K., and Mahadevan, S., "A New Approach to Estimate Discretization Error for Multidisciplinary and Multidirectional Mesh Refinement," *52nd AIAA/ASME/ASCE/AHS/ASC Structures, Structural Dynamics & Materials Conference*, AIAA 2011-1926, Denver, CO, 2011.

²⁷ Liu, Y., Chen, W., Arendt, P., and Huang, H.Z., "Towards a Better Understanding of Model Validation Metrics," *13th AIAA/ISSMO Multidisciplinary Analysis Optimization Conference*, AIAA 2010-9240, Fort Worth, TX, 2010.

²⁸ Ling Y. and Mahadevan S., "Integration of Structural Health Monitoring and Fatigue Damage Prognosis," *Mechanical Systems and Signal Processing*, Vol. 28, 2012, pp. 89-104.

ADDENDUM: Lab Task Summary

Quantifying Confidence in Model Predictions for Hypersonic Aircraft Structures

Benjamin P. Smarslok

*Air Force Research Laboratory, Aerospace Systems Directorate, Structural Sciences Center
Wright-Patterson AFB, OH, 45433*

LRIR #: 12RB10COR (Computational Math, Fahroo) and 12RB05COR (Structural Mechanics, Stargel)

Reporting Period: 10/1/2011 – 9/30/2013

Lack of confidence in structural response and life predictions of a vehicle exposed to combined extreme environments has consistently prevented the USAF from fielding affordable, reliable, and reusable hypersonic space access platforms. Significant strides have been made in modeling complex interactions of the multi-physics, fluid-thermal-structural coupling applicable to hypersonic flow conditions. However, validation of these models remains a challenge due to limited experimental data for hypersonic conditions. This research addresses fundamental and critical issues in quantifying uncertainty and assessing the confidence in model predictions of hypersonic structural response through a systematic framework. The framework will provide the capability to quantify the model prediction confidence, enabling its use as a decision-making metric for model fidelity selection and determining the necessary level of coupling in the modeling of an aerothermoelastic system. The first phase of this research effort focused on developing a model uncertainty framework for the aerothermal components of the coupled system. The modeled conditions correspond to aerothermal test data from hypersonic wind tunnel experiments of a spherical dome protuberance on a flat plate. Local and global sensitivity analyses were employed to investigate the sensitivity of model predictions to the input variables. A Bayes network was constructed for aerodynamic pressure and heating to integrate model predictions, aerothermal data, and various sources of uncertainty. Bayesian model calibration was performed with the test data to quantify uncertain model parameters and errors. Finally, a Bayesian hypothesis testing-based confidence metric was used to compare the accuracy of aerodynamic pressure predictions for different forms of piston theory.